Solar System Research, Vol. 39, No. 2, 2005, pp. 85–101. Translated from Astronomicheskii Vestnik, Vol. 39, No. 2, 2005, pp. 99–116.

Morphology and Geological Structure of the Western Part of the Olympus Mons Volcano on Mars from the Analysis of the *Mars Express* HRSC Imagery

A. T. Basilevsky[1], G. Neukum[2], B. A. Ivanov[3], S. K. Werner[2], S. van Gesselt[2], J. W. Head[4], T. Denk[5], R. Jaumann[5], H. Hoffmann[5], E. Hauber[5], T. McCord[6], and the HRSC Co-Investigator Team

[1]*Vernadsky Institute of Geochemistry and Analytical Chemistry, Russian Academy of Sciences, ul. Kosygina 19, Moscow, 119991 Russia*

[2]*Institute of Geosciences, FU Berlin, Malteserstr. 74-100, Bldg. D, 12249 Berlin, Germany*

[3]*Institute of Dynamics of Geospheres, Russian Academy of Sciences, Leninskii pr. 38-6, Moscow, 117334 Russia*

[4]*Department of Geological Sciences, Brown University, Providence, RI 02912, USA*

[5]*DLR-Institute for Planetary Studies, Rutherfordstr. 2, 12489 Berlin, Germany*

[6]*Hawaii Institute of Geophysics and Planetology, University of Hawaii, 2525 Correa Doad, Honolulu, HI 96822, USA*

Received September 28, 2004

Abstract—The images of the western part of Olympus Mons and adjacent plains acquired by the HRSC camera onboard the *Mars Express* spacecraft were studied. The morphology, topography, and color of the surface were investigated. The surface age was determined by the frequencies of impact craters. The examination of the HRSC images combined with an analysis of the MOC imagery and MOLA altitude profiles have shown that the Olympus Mons edifice, at least in its western part, is composed of not only lavas but also of sedimentary and volcanic–sedimentary rocks consisting of dust, volcanic ash, and, probably, H_2O ice that precipitated from the atmosphere. These data also indicate that glaciations, traces of which are known on the western foot of Olympus Mons (Lucchitta, 1981; Milkovich and Head, 2003), probably also covered the gentle upper slopes of the mountain. It is probable that the ice is still there, protected from sublimation by a dust blanket. Confirming (or rejecting) its presence is a challenge for the scheduled radar sounding with the MARSIS instrument mounted on the *Mars Express* spacecraft as well.

INTRODUCTION

The High-Resolution Stereo Camera (HRSC) is a part of the scientific payload for the European Space Agency's (ESA) *Mars Express* spacecraft, which has been operating on the orbit of Mars. The camera acquires images in nine CCD lines (with 5184 sensor elements each) by scanning the Martian surface while the spacecraft is in motion in the orbit. The five lines viewing the surface through panchromatic filters yield a series of simultaneous stereo images. The four lines receiving the image through blue, green, red, and infrared filters give information on the surface color. From an altitude of 250 km, one pixel of the image corresponds to an area of 10×10 m, and the image swath is 52 km. The camera characteristics can be found in more detail in the paper by Neukum and Jaumann (2004).

The images under consideration were taken during orbit 143 on February 24, 2004 at about 13^h25^m LT, when the Sun was 65°–70° above the horizon. The altitude of the spacecraft was about 275 km, which provided a maximal image resolution of ~11 m per pixel. We analyzed images obtained through color filters, stereo images as a two-color anaglyph, and a digital terrain model built from the stereos. In addition, the MOLA altimetry and the imagery acquired in the *Mars Global Surveyor* mission from the narrow-angle MOC camera were invoked as needed. The studied area is bounded by the coordinates 13°–24° N and 220°–224° E. It includes the western part of Olympus Mons and the westward adjacent lowland plains. Preliminary results of the HRSC data analysis for this region of Mars and for some others are briefly described in the works by Neukum *et al.* (2004), Head *et al.* (2004), Hauber *et al.* (2004), and Murray *et al.* (2004). Here, we present the results of a more thorough analysis of the data received during revolution 143.

Olympus Mons is the highest volcano on Mars: it rises more than 21 km above the mean level of the planetary surface (Fig. 1). Its diameter is about 600 km. On the summit, there is a caldera about 80 km across, with the traces of several collapse episodes detectable. At altitudes from 6–8 km to the summit, the surface is gently convex, which suggests that this volcano is a shield type. On almost all sides, Olympus Mons is surrounded by a scarp 6–8 km in height. To the north and west of the volcano, on the adjacent lowland plains, there are highly fractured areas. This is the so-called Olympus Mons aureole, which resulted from the fall and sliding of the mountain slopes under gravity (Harris, 1977;

0038-0946/05/3902-0085

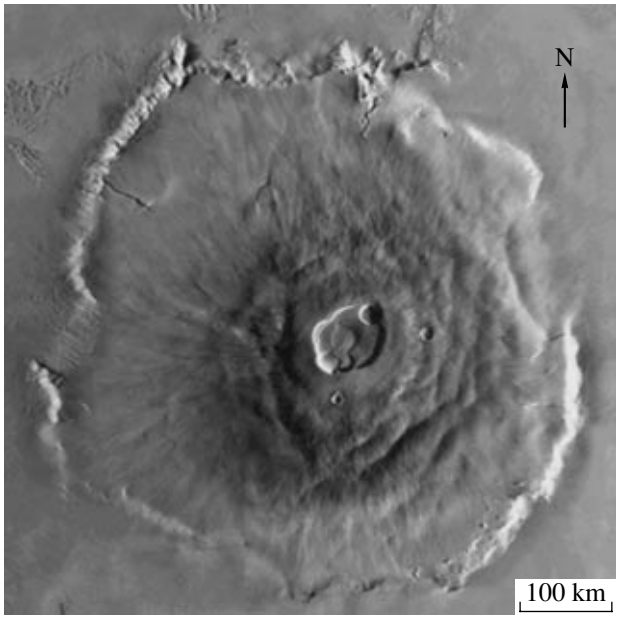

Fig. 1. The Olympus Mons edifice on Mars. The area under study: the western part of the volcano and the adjacent plain. The hummocky terrain to the north and west of the volcano is the so-called "Olympus aureole." Image from a wide-angle MOC camera. JPL/NASA/Malin Space Science Corporation.

Lopes *et al.*, 1982). Since the early 1970s, when Olympus Mons was found in the *Mariner 9* images, it has been considered a volcanic construct composed of basaltic lava accumulations (Carr, 1973; Greeley and Spudis, 1981). Our analysis of the HRSC imagery suggests a more complicated geologic history of this edifice, at least in its western part, with the interplay of basaltic volcanism and several other processes.

SURFACE MORPHOLOGY

There are three major morphological elements in the studied region: (1) the western part of the mountain summit, which is rather flat here, and, consequently, hereafter called the "summit plateau"; (2) the western slope scarp; and (3) the lowland plains, among which the pieces of the Olympus Mons aureole are seen on the north of the territory (Fig. 2).

Summit Plateau

As follows from the digital terrain model, the surface altitudes vary here from ~7 to 9.7 km above the mean level of the planet, with the highest values in the east, closer to the summit. The studied part of the plateau is rimmed on the north, west, and south by steep (20°–35°) to gentle (4°–10°) slopes (HRSC and MOLA data). In the southern and central parts of the plateau, numerous *lava flows* are seen (Fig. 3). The HRSC images show that, as a rule, the flows are rather long (up to 10–20 km) and narrow (0.5–2 km), usually with levees. In the MOC images of the same area made with a resolution of 3–6 m, it is seen that some of these flows are even narrower, namely, 200–300 m. They are approximately radial to the volcano center. The surface slopes within the lava fields on the plateau range from 30 to 70 m/km. No evident lava sources like craters or fissures are seen.

In the northern part of the plateau, lava flows are rarely observed (Fig. 4). The surface is mostly smooth there with an alternating system of brighter and darker spots and streaks. Similar spots and streaks, however, superimposed on the lava flows, are also typical of the southern and central part of the plateau. In the south of the plateau, the streaks are close to radial to the edifice summit. Further to the north, they are more northward-trending with azimuths NNW 340°–350° in the northern part of the plateau. Most likely, these streaks are aeolian features, and their orientation corresponds to the directions of currently prevailing winds. There are also impact craters of tens to hundreds meters across that occur on the plateau rather often. Their number per unit surface area was used for an estimation of the surface age (see below).

Along the western edge of the plateau, there are several *mesas*—hills or mountains with flat summits and steep slopes—from several kilometers across to 15 × 50 km (Fig. 2). We will describe the three largest.

At the boundary between the northern and southern parts of the plateau, there is a planimetrically polygonal 15 × 50 km mesa in the northwestern–southeastern direction. The coordinates of its center are approximately 20.7° N and 222.5° E. The western part of the mesa is shown in Fig. 5. It is seen from the figure that the steep (30°–35°) western slope of the mesa, which is simultaneously the upper part of the summit plateau scarp, is composed of horizontally layered deposits cut with numerous branching ravines. The northern and southern slopes seen in the figure are also steep but relatively low (300–500 m). There are also ravines in this area, but they are not branching. On the mesa top, steps, evidently suggesting the layering of the material of the upper part of the mesa, are seen. The layering is also noticeable in the fragments of the MOC image made with a resolution of 4.5 m (Fig. 5). The apparent thickness of the thinnest layers distinguishable in the MOC image is 1–2 pixels (4.5–9 m), which gives an actual thickness of about 3–6 m, if a slope steepness of 30°–35° is taken into account. In the HRSC and MOC images, the layering can be traced downslope for about 1 km in altitude. On all sides of the mesa, the highest part of the slope is noticeably gentler (~15°–20°). Its horizontal width is 300–400 m, and, in the MOC image, two horizontal layers of small thickness (several meters) are seen at the very top of this part of the slope. The MOC image shows also linear dunes 15–20 m in width and 100–150 m in length in some places on the summit surface of the mesa.

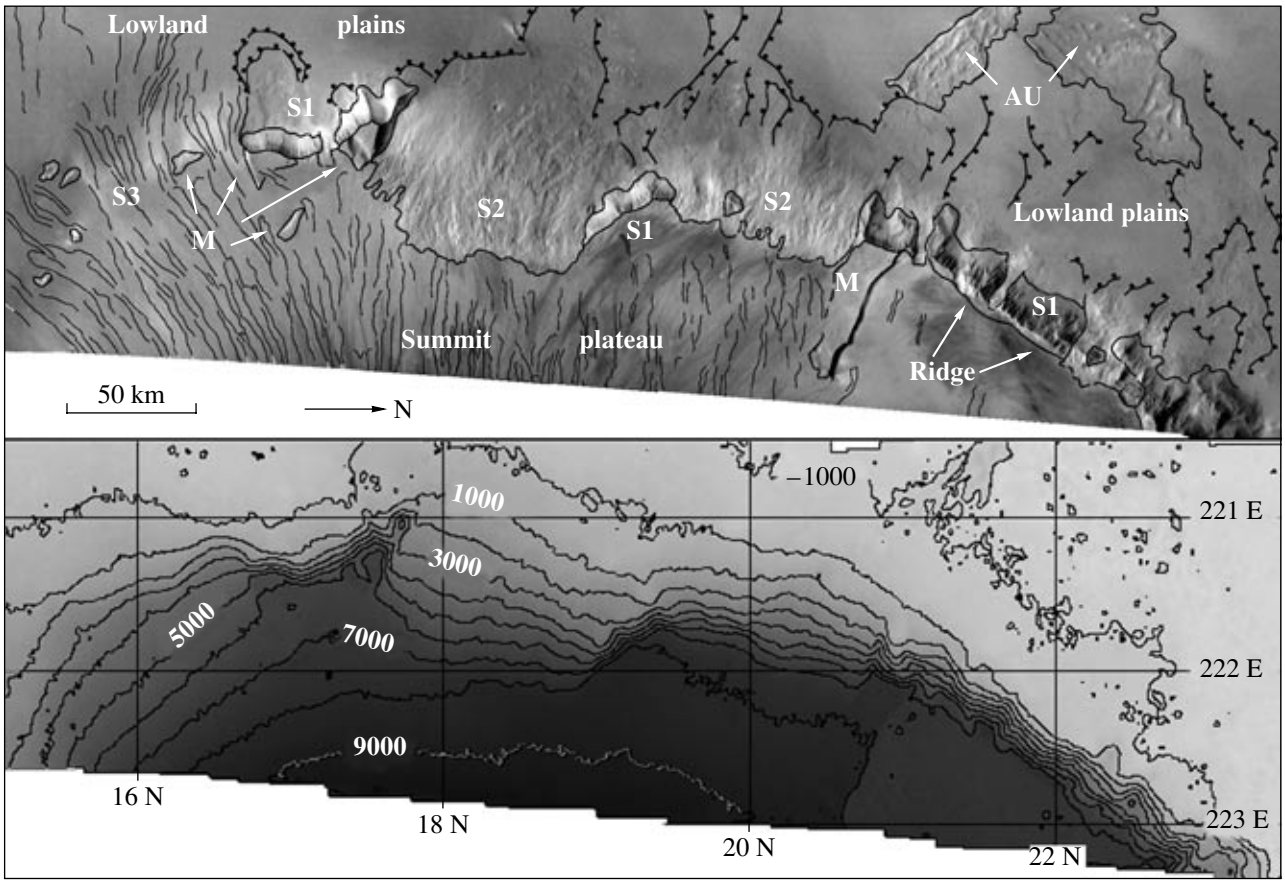

Fig. 2. The area of investigations. Top: the HRSC image; bottom: the map of surface altitudes composed of stereo measurements in HRSC images. Legend: S1, S2, and S3: the slopes of type 1, 2, and 3 respectively; M: mesas; AU: areas of the Olympus aureole; thin lines: the borders of lava flows; thick lines with points: glacial-type lobate flows.

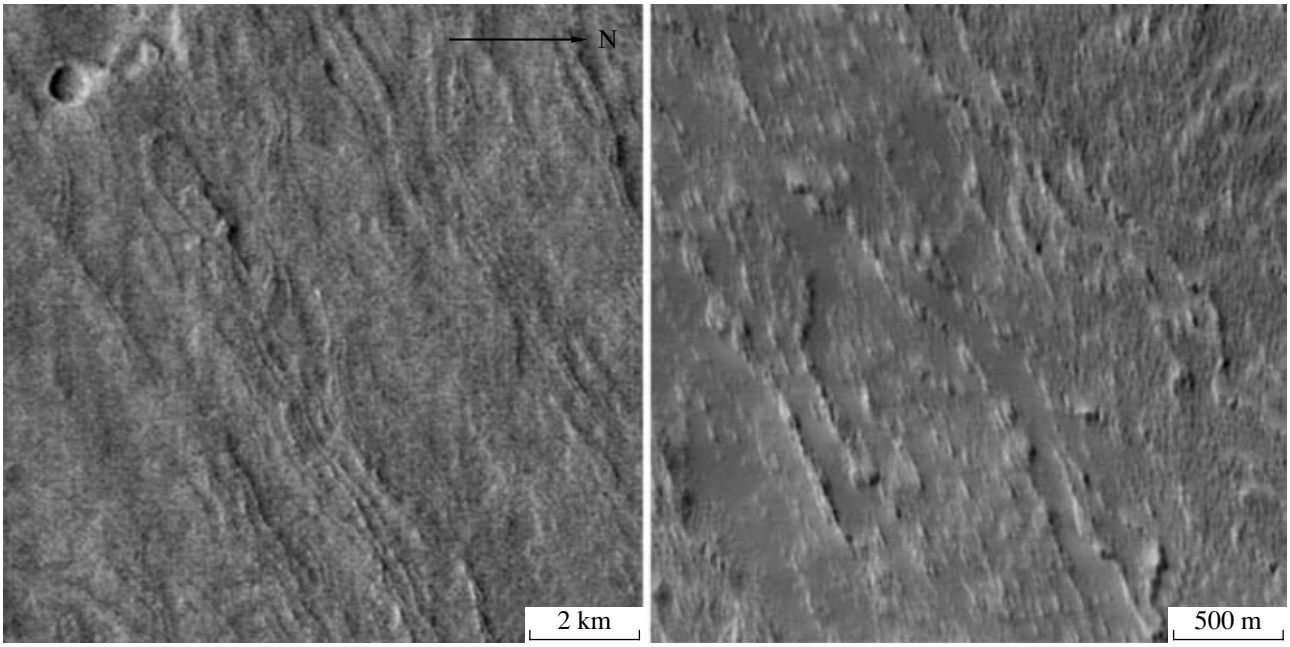

Fig. 3. Lava flows in the southern part of the summit plateau. The fragments of the HRSC (left) and MOC E08-01706 images (right).

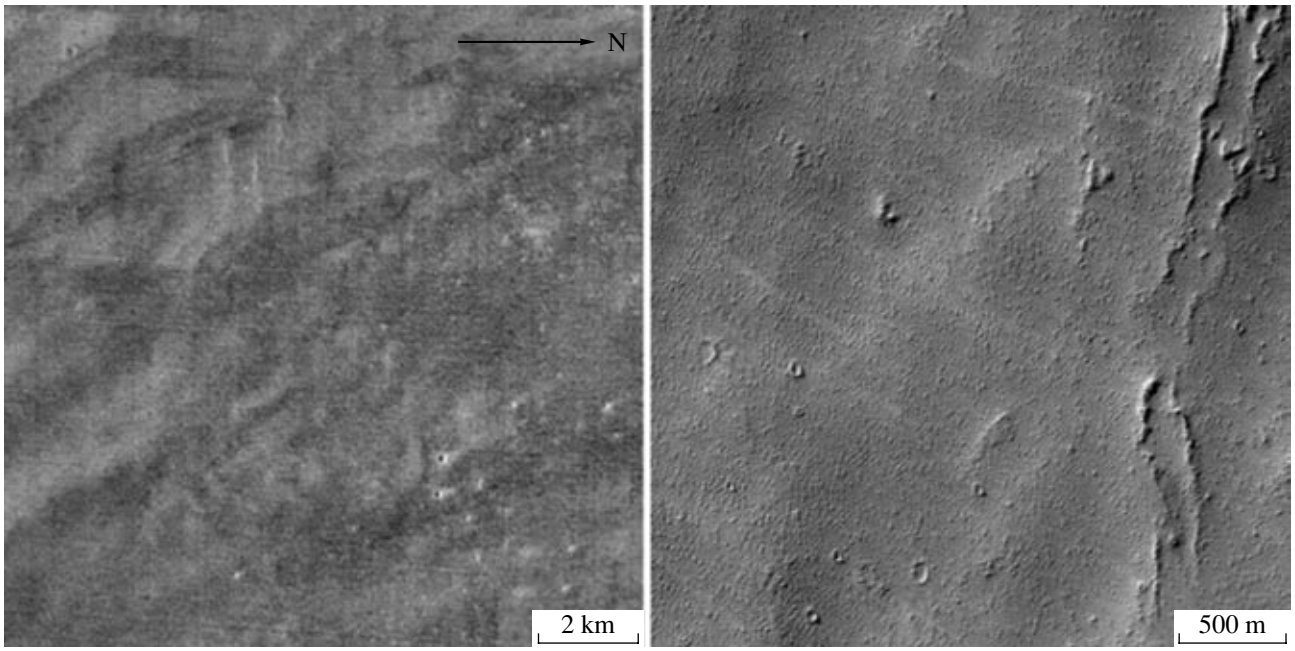

Fig. 4. The surface of the northern part of the summit plateau. The lava flows are rare. The fragments of the HRSC (left) and MOC E09-01693 images (right).

At the boundary between the central and southern parts of the plateau, there is a planimetrically pentagonal mesa 11×16 km in size and centered approximately at 17.5° N and 221.3° E (Fig. 6). Its slopes are steep, namely, up to 30°–35° in the upper part. The north-northeastern, northwestern, and southwestern slopes, which are simultaneously the upper parts of the general scarp of the summit plateau descending by several kilometers, are covered with branching ravines. The ravines on the northeastern and southeastern slopes, which are several hundred meters high and border the adjacent summit plateau areas, are not branching. The surface of the mesa summit is complicated, with several shallow (tens of meters) and deep (almost down to the level of the adjacent summit plateau areas) depressions. In the HRSC images, the surface of the mesa summit between the depressions appears to be smooth and relatively bright. In the MOC image with a 3-m resolution, which covers a part of the mesa summit and a part of its southwestern slope (Fig. 6), numerous dunes 20–50 m long and isometric hummocks of approximately the same size are seen on the summit surface. The same image clearly shows the upper gentle part of the mesa slopes and the layering on the base and extreme top of this part. The minimal apparent thickness of the layers is 1–2 pixels (3–6 m), which suggests an actual thickness of about 2–4 m with the slope steepness accounted for. On the gentle part of the slope, dunes and hummocks are also observed. In the HRSC and MOC images, the layering can be traced down along the north-northeastern, northwestern, and southwestern slopes for about one vertical kilometer.

In the southern part of the summit plateau, there is a triangular 15×20 km mesa centered approximately at 16.8° N and 221.4° E (Fig. 7). Its western slope is the upper part of the summit plateau scarp and is cut by branching ravines. Thin (meters, judging by the MOC images) horizontal layering is seen in its upper part (about 1 km in height). The southern slope is moderate in height and is complicated with nonbranching ravines. Its foot is a surface of the summit plateau with lava flows. The northeastern boundary of the mesa is a slope only in its northern and southern parts. In its central part, the surface of the adjacent area of the summit plateau is elevated relative to the mesa surface, and the plateau lava flows enter into the mesa. The mesa surface becomes rough here, as if the material of its upper layer collapsed upon contact with lava. Similar phenomena are described by Squyres *et al.* (1987) and Ivanov and Head (2003) for the case when lava entered the areas with a high content of ice in the surface rocks. On the north of the mesa, a 1.4×1.8 km oval crater is seen. Its interior slopes are very steep, which makes it resemble a fresh impact crater. However, contrary to the case of fresh impact craters, it has neither an elevated rim nor ejecta. Probably, this is a result of a collapse, which suggests a partial removal of the subsurface material.

The northern part of the summit plateau is rimmed by *a ridge* standing several hundred meters above the adjacent plateau areas (Fig. 8). The western slope of the ridge is the upper part of the general edifice slope, and is cut by numerous branching ravines. The eastern slope of the ridge, supported by the summit plateau sur-

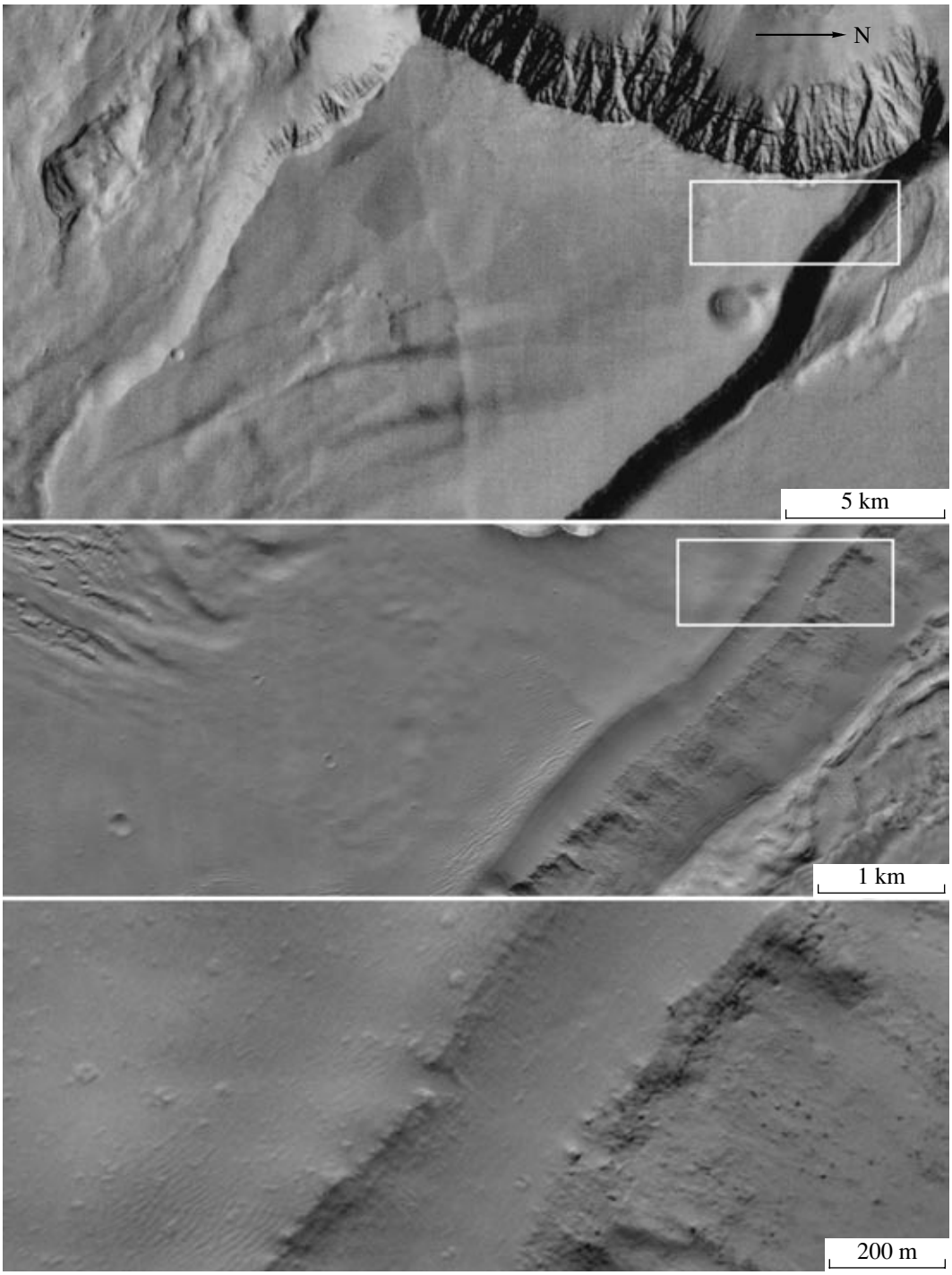

Fig. 5. The western part of the mesa at 20.7° N, 222.5° E. The HRSC image (top) and the fragments of the MOC E04-01135 image (center and bottom).

face, has a smooth unravined surface, which is relatively bright as a rule. The ridge, at least in its upper part (not less than one vertical kilometer), is composed of layered deposits, which look like the layered deposits of mesas. The ridge is broken by breaches, which are the upper parts of wide (from 3–4 to 10–12 km) valleys going down the slope of the mountain.

In one of the breaches, at ~21.55° N, *a lobate flow* 4×8 km in size commences (Fig. 9). The frontal zone of the flow is rimmed by gently sloping ridges, and this flow resembles glacial flow remnants in morphology. The flow pattern and altitude distribution in this area indicate that the flow moved to the southeast and southwest from the ridges into the summit plateau.

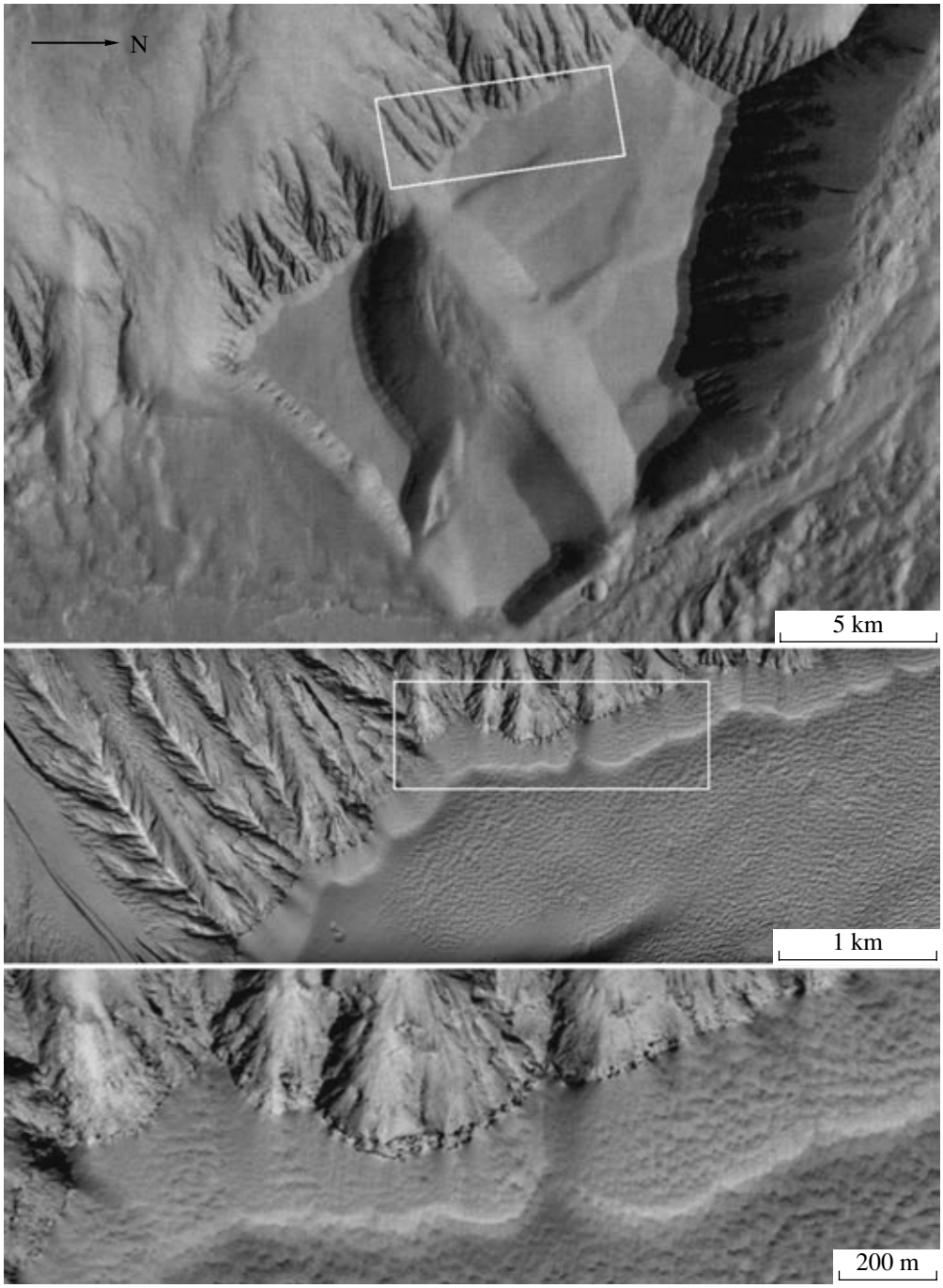

Fig. 6. The mesa at 17.5° N, 221.3° E. The HRSC image (top) and the fragments of the MOC E05-02498 image (center and bottom).

The Western Slope Scarp of Olympus Mons

The western slope scarp of Olympus Mons consists of slopes that can be subdivided into three morphological types (Fig. 2).

The slopes of type 1 have a steep (up to 30°–35°) upper part dissected by branching ravines, while their lower part is gentler and smoother (Fig. 10). Slopes of this type are mostly widespread in the northern part of the studied area, where the summit plateau is rimmed by the ridge. Moreover, such slopes occur in the central part and at the boundary between the central and southern parts of the studied terrain, sometimes in the region of the mesas described above and sometimes away from mesas, where the summit plateau borders the scarp. The branching ravines look similar to those in arid zones on the Earth, for example, in Death Valley in California (Fig. 11). These terrestrial ravines are cut by running water, which, however, does not imply that the

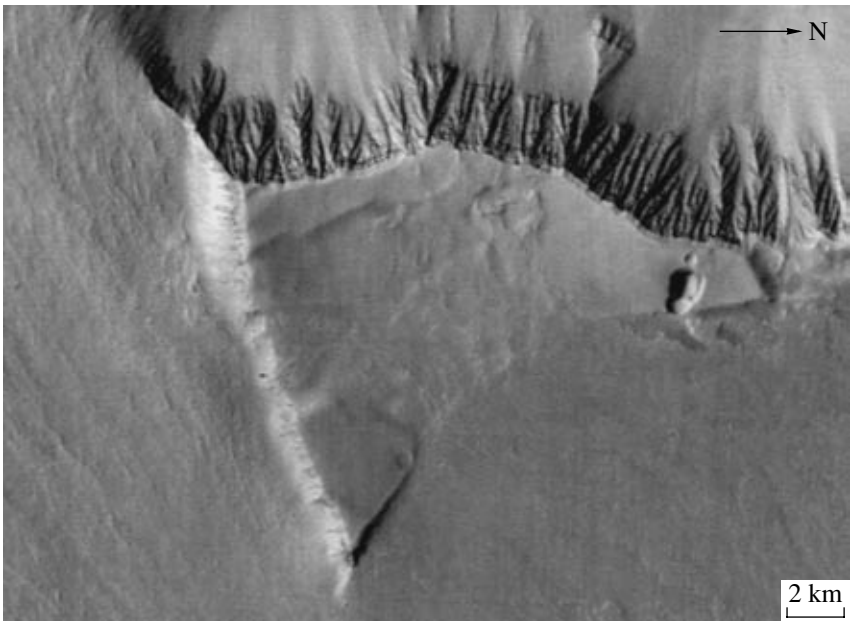

Fig. 7. The mesa at 16.8° N, 221.4° E. HRSC image.

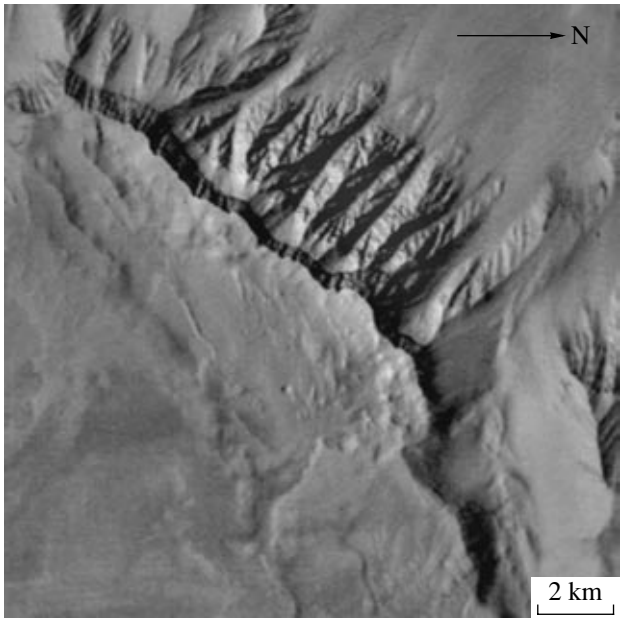

Fig. 8. The ridge fringing the summit plateau in its northern part. The valley with an U-shaped cross-section profile entering into the summit plateau surface is at the bottom right. HRSC image.

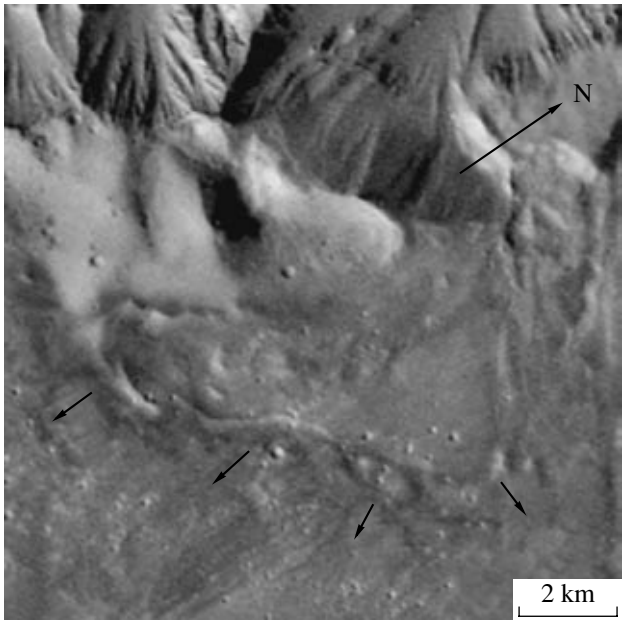

Fig. 9. The flowlike glacial-type landform is in the image center. A portion of the ridge is at the top left. The summit plateau surface is at the bottom. HRSC image.

ravines of the western scarp of Olympus Mons were also formed by running water. We found that, on the slopes of deep (several kilometers) tectonic valleys of Venus, where there is no liquid water on the surface, there are ravines very similar to those of Death Valley (Fig. 11). The lower smoother and gentler parts of the slopes of type 1 look very similar to the taluses of the lower parts of the slopes on the Earth and Venus (Fig. 11).

As has already been mentioned, there are several breaches in the ridge fringing the northern part of the summit plateau (Figs. 8 and 10). They are the upper parts of wide valleys intruding into the ridge and going down the mountain scarp. Sometimes, the head areas of the valley, having ploughed through the ridge, also enter into the surface of the summit plateau beyond the ridge (Fig. 8). The valleys have an approximately

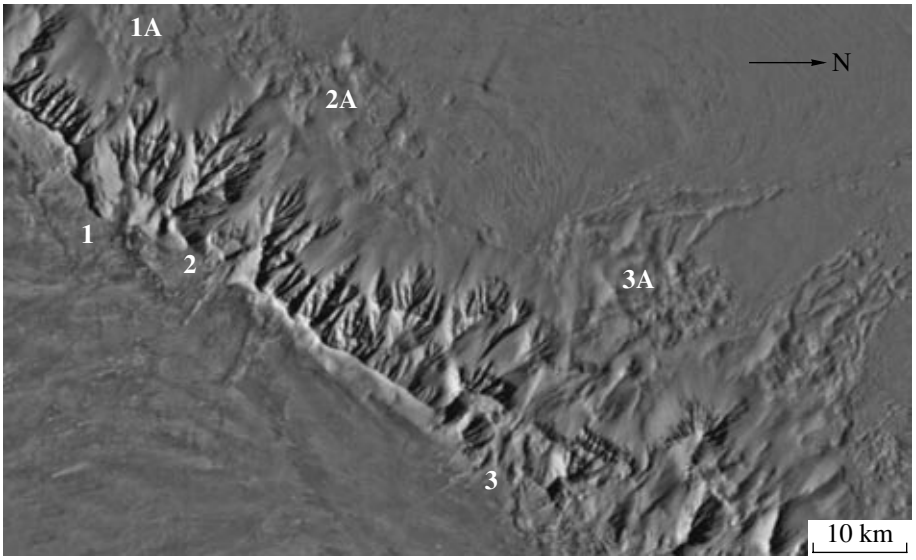

Fig. 10. The slope of morphological type 1 edging the northern part of the summit plateau. HRSC image. Notation: 1–1A, 2–2A, and 3–3A indicate, respectively, the location of the sources of glacial-type valleys and the hummocky hills below their mouths. The number 2 is placed in the region shown in Fig. 9.

U-shaped cross section. Each of these valleys ends at the scarp foot with a hill 10–20 km across and several hundreds of meters high. These hills have a chaotically hummocky surface, and their distal (in relation to the scarp) sides have lobate outlines fringed by concentric ridges. Such morphology of the valleys with associated piedmont hills evidently suggests that they are ploughed by glaciers, the source area of which was high on the summit plateau, and that the piedmont highlands are terminal moraines. Such an interpretation is also supported by the glacial-type lobate flow (Fig. 9) found high on the scarp in the breach of the fringing ridge (see above). At the foot of the type-1 slope, at the boundary with the type-2 slope (19.1° N, 221.6° E), there are two tonguelike flows (Fig. 12) that are interpreted to be debris-covered glaciers of the alpine type (Head *et al.*, 2004).

The slopes of type 2 are less steep: 8°–12° in the upper part and 3°–5° in the lower part. They are common in the central segment of the western scarp of Olympus Mons. Slopes of this type often start with a narrow (several kilometers) area of so-called etched terrain (Fig. 13). Typical of this zone are the usually flat-bottomed closed depressions observed against the plain terrain background. The depressions are irregular in shape and reach 2–4 km across. Sometimes, individual hills are observed to dominate the plain. The pattern of this terrain implies a loss of the surface material either by wind, in which case they are deflated depressions, or by sinking, in which case they are collapse-type depressions. The flat bottom of most of the depressions evidently excludes the second possibility. On the slopes of depressions and hills, steps are seen, which evidences the horizontal layering of the rocks composing this terrain (Fig. 14). Judging by the width of the benches in the places of the layer outcroppings, their minimal thickness is comparable to the HRSC image resolution (11–22 m) and, consequently, may be smaller. We failed to find the MOC images on these outcrops of layers, but, judging by their elevation, they are the same layers that are seen in the upper part of the mesa and ridge slopes, and their thickness is about several meters.

Downslope from the etched terrain zone or in direct contact with the summit plateau are observed complex irregular depressions several kilometers across; they resemble "chaoses" observed in the source areas of the Martian channels of catastrophic outflow (Fig. 15). Chaoses are believed to be collapse depressions formed due to the release of subsurface water, which then ploughed these channels; the melting of ground ice by magma intrusion could be one of the variants of water mobilization (Baker, 1982; Baker *et al.*, 1992). For the chaoses of the western Olympus scarp, it could be the intrusions of dikes extending from the magma chamber of the volcano. In one of the few MOC images of this area, thin horizontal layers, similar to those observed in the scarps of mesas and the fringing ridge, are seen on the slopes of the chaotic-type depression (Fig. 16). It is important to note that the outcrops of layered rocks here and in some other places of the type-2 slopes are cut by parallel groves of the yardang type, which very often indicates mechanically soft rocks (Greeley and Iversen, 1985).

On the type-2 slopes, in association with the chaoses, sinuous channels several hundred meters wide and several kilometers long are often observed (Fig. 15). The channels of such morphology are believed to be cut by fluid flows. In the case of Mars, the flow of water is usually discussed (Carr, 1996). The downslope-trending chains of rimless craters occur in some places here (Fig. 17); they are also commonly considered to be collapse depressions.

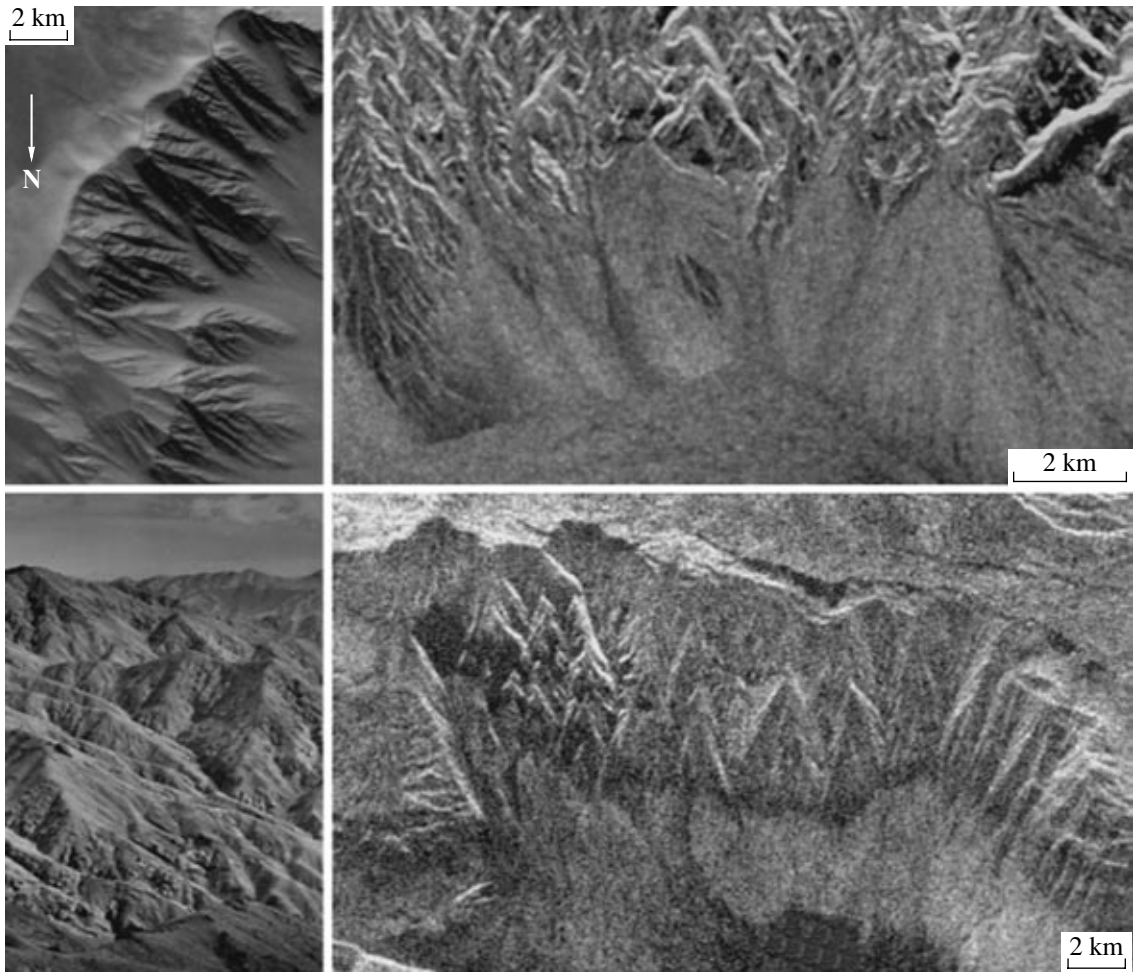

Fig. 11. The ravines on the type-1 slope of the western scarp of Olympus Mons (top left) in comparison with the ravines on the Earth and Venus. The ravines on the slope of Death Valley in California: a perspective photo from the air (bottom left, from http://libraryphoto.er.usgs.gov/parks1.htm) and a radar image made by Spaceborne Imaging Radar-C/X-Band, 1994 Space Shuttle missions (top right, from http://photojournal.jpl.nasa.gov/catalog/PIA01349). The ravines on the slope of the Devana Chasma rift on Venus (bottom right, the fragment of the *Magelan* F-MAP).

The slopes of type 3 are generally the least steep: from 3°–5° to 7°–9°. They contain neither ravines nor flat-bottom depressions typical of etched terrain, chaotic depressions, channels and rimless crater chains, or tonguelike flows. They are covered with downslope-descending lava flows, which continue for 10–30 km into the lowland plains (Fig. 18); these flows are similar to those on the summit plateau (Fig. 3). The type-3 slopes are commonly present in the south of the area under study (Fig. 2).

Lowland Plains

The lowland plains, as follows from their name, are mostly below the mean altitude level of the Martian surface. They are represented by three morphologic types.

The plains of type 1 occur along the western boundary of the studied terrain. They have practically no visible landforms in the HRSC images; only rare impact craters with diameters of tens to several hundreds of meters are seen (Fig. 19).

The plains of type 2 develop at the foot of the slopes of type 1 and 2. Typical of them are lobate flows with concentric ridges of flowing (Fig. 20). They were discovered in the *Viking* images and were interpreted as glacial deposits (Lucchitta, 1981). Other interpretations have also been suggested: the lava flows of an ancient larger volcano (Carr *et al.*, 1997), pyroclastic flows (Morris, 1982), deposits of the landslides from the Olympus Mons scarp (Lopes *et al.*, 1982), and deposits of landslides involving ice grease (Tanaka, 1985). The recent analysis of these flows on the basis of the *Mars Global Surveyor* and *Mars Odyssey* imagery has confirmed the glacial hypothesis and has adjusted it to be due to debris-covered piedmont glaciers (Milkovich and Head, 2003). In the HRSC images combining a rather high resolution and a large coverage, it is possible to distinguish several phases in the formation of

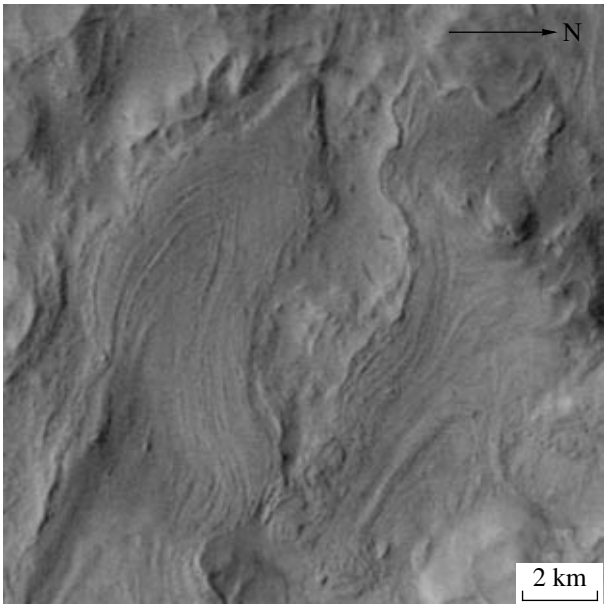

Fig. 12. The tonguelike flows of the alpine-glacier type at the base of the type-1 slope. HRSC image.

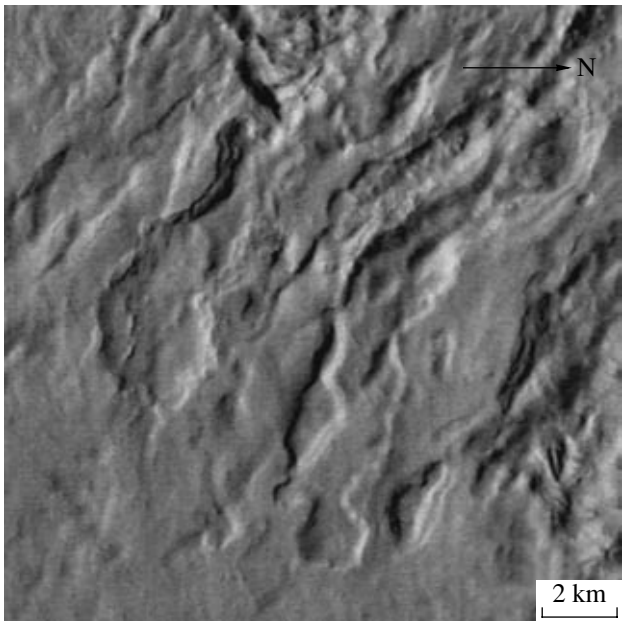

Fig. 13. The etched terrain at the upper part of the slope of type 2. HRSC image.

these deposits, which is also confirmed by the estimates of the surface age made from the frequencies of the superimposed impact craters (see below).

The plains of type 3 occur at the foot of the type-3 slopes covered with lava flows, and there are also lava flows in these areas (Fig. 18). The flows are, in general, of the same type as those on the upper slope and summit plateau. However, in the transitional zone between the slope and piedmont plain, it is seen that the flows are systematically wider in the plain, probably due to a lower flow velocity at smaller slopes.

THE SURFACE COLOR

The images obtained through four filters—blue (430 ± 45 nm), green (530 ± 45 nm), red (750 ± 20 nm), and infrared (970 ± 20 nm)—were calibrated and then used for determining the color ratios 430/750 nm, 530/750 nm, and 970/750 nm, i.e., the ratios of the brightness in the blue, green, and infrared ranges to the brightness in a red range. For calibration, the spectra measured in ground-based telescopic observations (McCord *et al.*, 2004) and cross-calibration to the OMEGA experiment data (Bibring *et al.*, 2004) were invoked. The measurements were done for 16 terrain types: (1) the bright areas of the summit plateau; (2) the summit plateau areas intermediate in brightness; (3) the dark areas of the summit plateau; (4) the bright edge of the plateau; (5) the fringing ridge; (6) the dark regions of the slopes of type 1 with ravines; (7) the brightened regions of the type-1 slopes with ravines; (8) the smooth lower part of the type-1 slopes; (9) the piedmont hills; (10) the type-2 slopes—chaoses and channels; (11) the type-2 slopes between the chaoses and channels; (12) the bright and intermediate-brightness glacial-type flows on the plains; (13) the dark glacial-type flows on the plains; (14) the smooth plains; (15) the lava flows of the southwestern slope; (16) the lava flows of the slope base (see table).

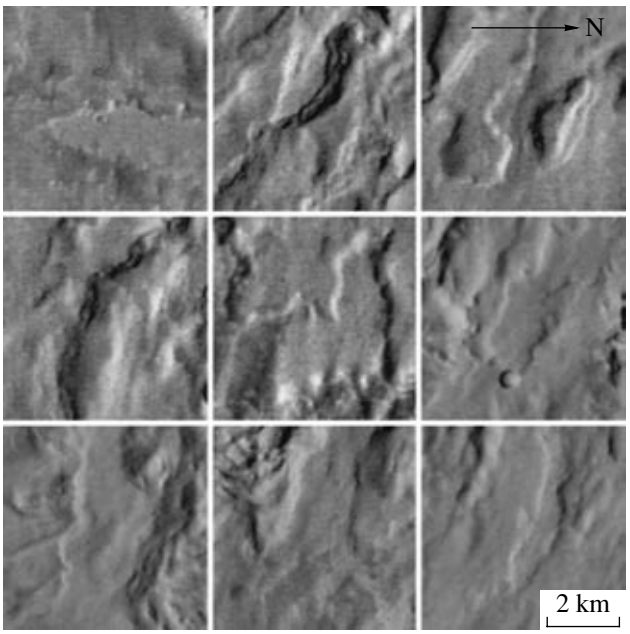

Fig. 14. Examples of layering observed in the upper part of the type-2 slopes. Fragments of the HRSC images.

The measurements showed that the variations in measured brightness are small: in each range, the high-

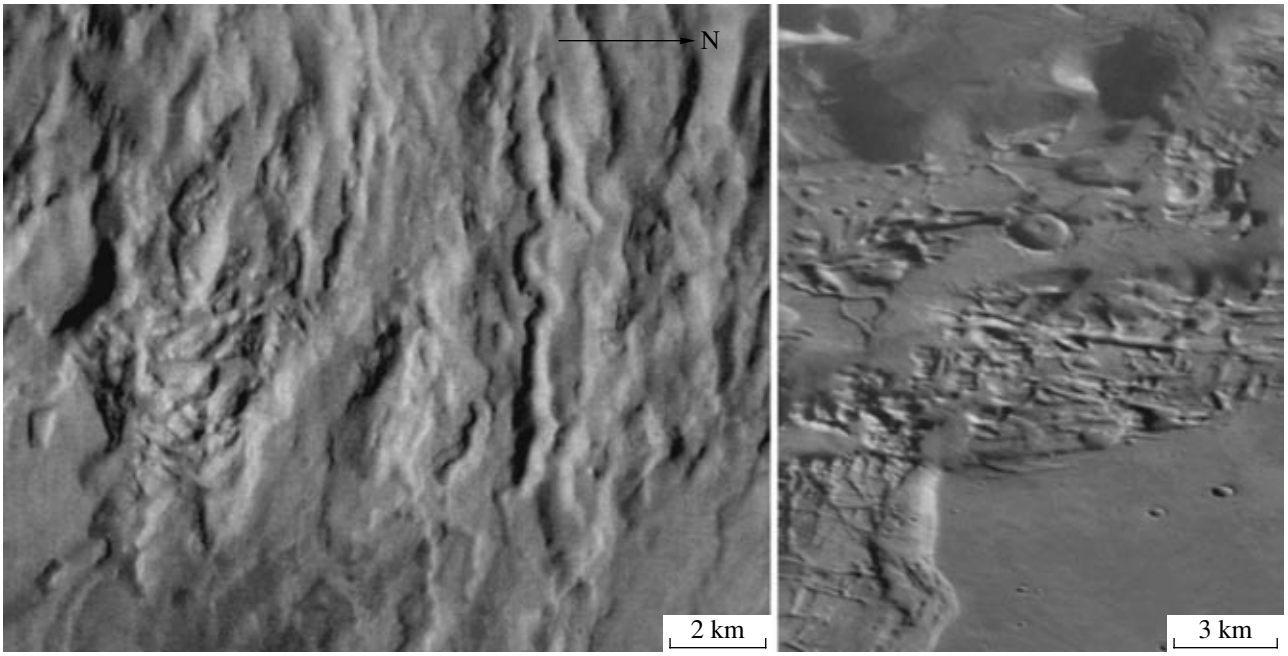

Fig. 15. Left: HRSC image (orbit 143) showing the chaos-type depression at the type-2 slope (in the left part) and a fluvial-type channel (in the right part). Right: HRSC image (orbit 520) showing the chaos in the source of Dao Vallis in the southern hemisphere of Mars.

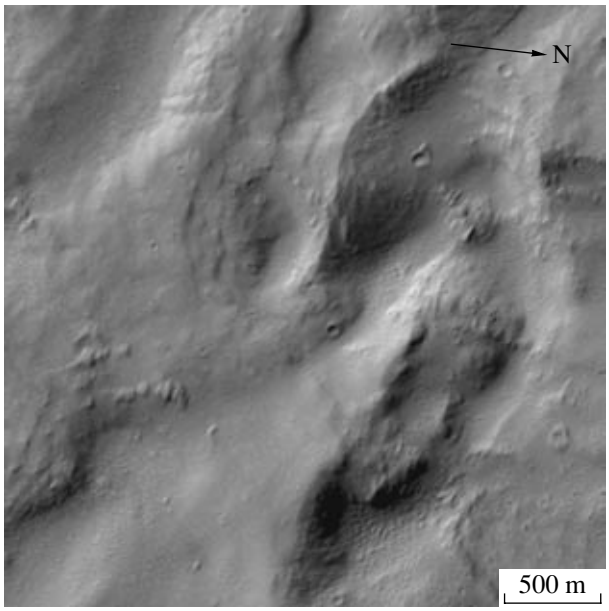

Fig. 16. Thin horizontal layers with yardang-type grooves on the slopes of chaos-like depressions at 18.7° N, 221.9° E. Fragment of the MOC E09-02639 image.

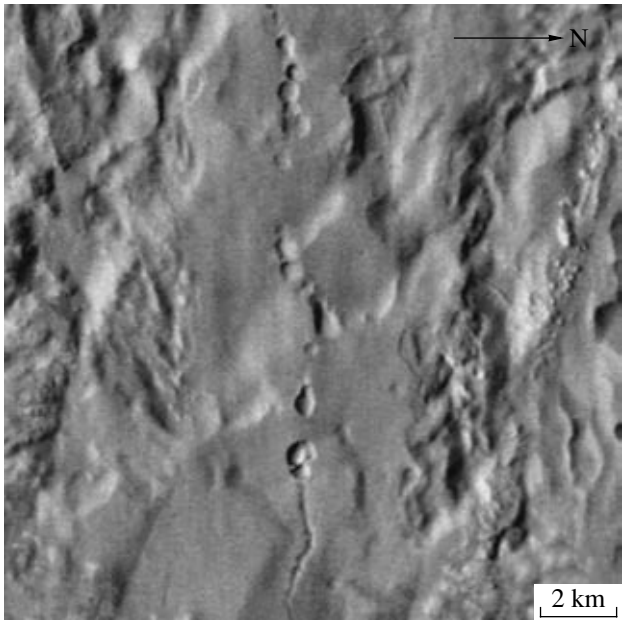

Fig. 17. The chain of rimless craters on the type-2 slope. HRSC image.

est and lowest values differ only by a factor of not more than 1.5. Naturally, the color ratios for various terrain units differ slightly or are practically the same (see table and Fig. 21). For the most studied types of terrain, they coincide with the values measured earlier for the bright regions of Mars. These regions are known to be covered with bright dust (Banin *et al.*, 1992). It is evident that almost everything observed in the studied area is also dust-covered. This inference agrees well with the data from the TES instrument that indicates a very low thermal inertia for the most part of Olympus Mons (Mellon *et al.*, 2000). A slightly higher inertia was

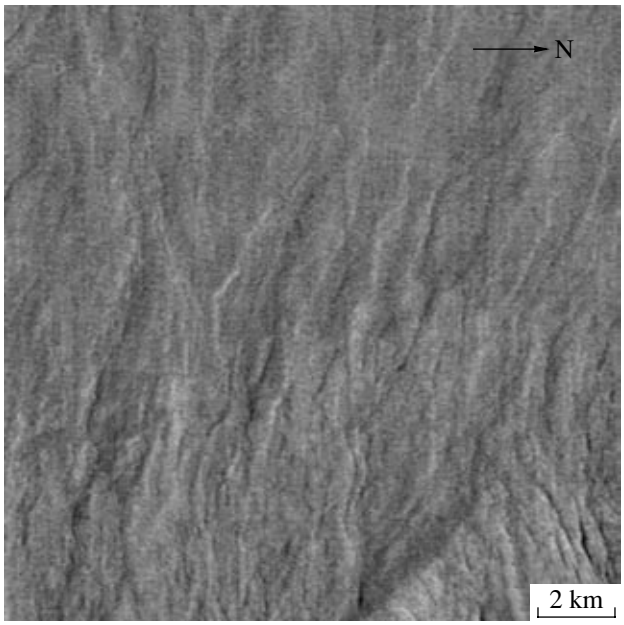

Fig. 18. The lava flows in the bottom of the type-3 slope and on the adjacent lowland plains. The boundary between the slope and plains is approximately in the middle of the imaged area and is traced by a noticeable increase of the flow width on the plain. HRSC image.

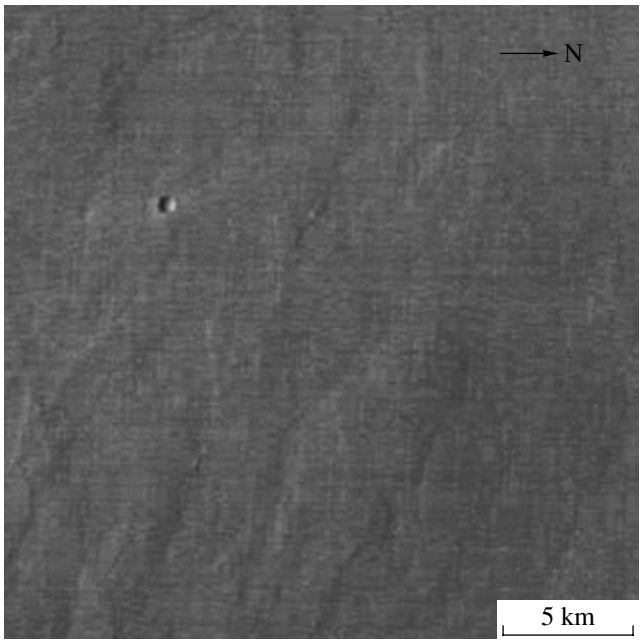

Fig. 19. The smooth plains with rare impact craters in the southwestern part of the studied terrain. The remnants of the lava flows occasionally entering the plains are seen at the bottom of the image. HRSC image.

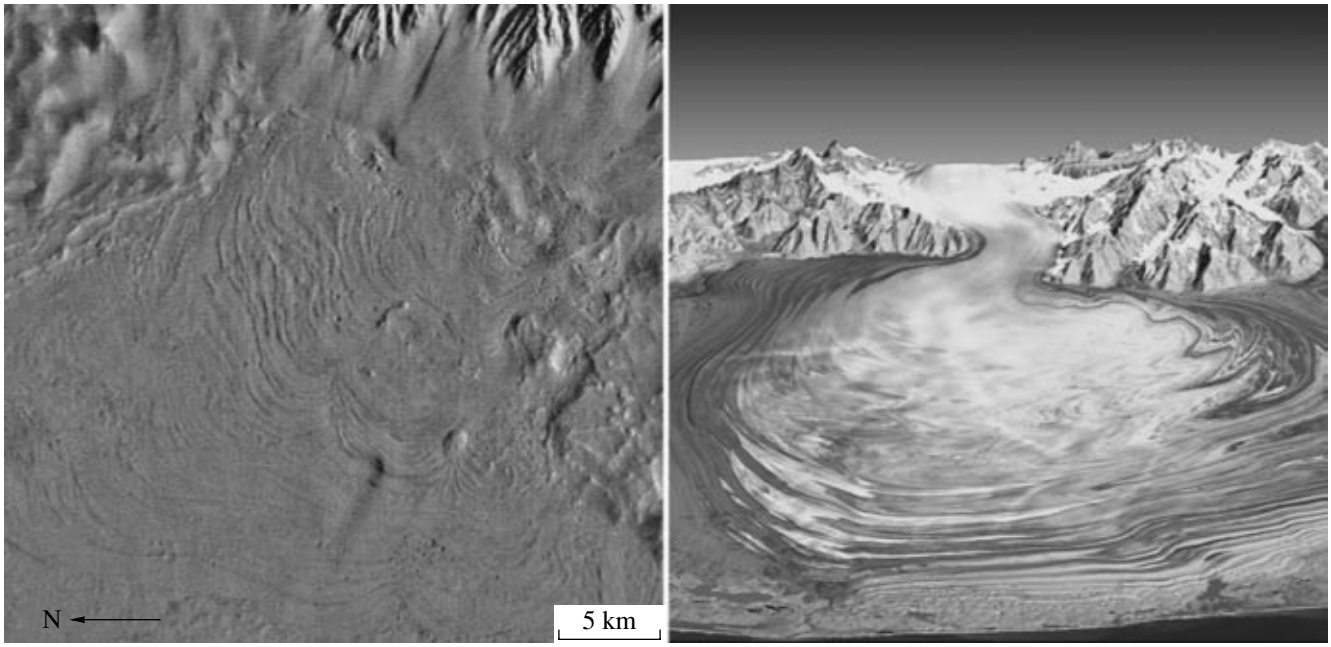

Fig. 20. Left: the lobate flows with ridges of flowing on the lowland plains under the northern part of the western scarp of Olympus Mons (HRSC image). Right: Malaspina Glacier, Alaska (http://photojournal.jpl.nasa.gov/jpeg/PIA03386).

obtained only for the scarp edging the edifice, where the amount of dust on the steep slopes must be less.

It is worth noting the following two distinctions. (1) The dark areas of the slopes of type 1 with ravines are characterized by the lowest ratios 970/750 nm, which is probably caused by the pyroxene absorption band in the near-infrared range (Pieters *et al.*, 1993). Pyroxene is contained in the basalt lava material or basalt ash outcroppings on the steep slopes of ravines, where there is less dust. (2) The surface of almost the

The average values and standard deviations of brightness (in DN's) in a red spectral range and color indices for various terrain types in the western part of Olympus Mons and the adjacent plains

No.	Terrain type	Number of measurements	Brightness in a red range		Color ratio 440/750 nm		Color ratio 530/750 nm		Color ratio 970/550 nm	
			Average	Standard deviation	Average	Standard deviation	Average	Standard deviation	Average	Standard deviation
1	Bright summit plateau	26	211.58	5.64	0.153	0.004	0.362	0.004	1.024	0.012
2	Intermediate summit plateau	18	191.83	7.49	0.157	0.005	0.361	0.005	1.007	0.006
3	Dark summit plateau	13	180.88	6.83	0.157	0.003	0.357	0.004	0.991	0.015
4	Bright plateau edge	54	221.59	9.05	0.156	0.003	0.365	0.004	1.012	0.016
5	Fringing ridge	20	211.01	13.27	0.162	0.003	0.373	0.009	1.012	0.035
6	Dark slope with ravines	16	191.21	15.76	0.16	0.01	0.36	0.01	0.955	0.029
7	Bright slope with ravines	30	198.6	15.02	0.158	0.005	0.363	0.007	0.987	0.033
8	Smooth slope	33	204.15	16.11	0.162	0.006	0.376	0.006	1.028	0.025
9	Piedmont hills	13	196.38	4.29	0.169	0.005	0.385	0.005	1.044	0.014
10	Chaoses and channels	17	218.88	8.74	0.159	0.003	0.368	0.003	1.013	0.016
11	Between chaoses and channels	14	211.75	7.15	0.159	0.004	0.368	0.007	1.015	0.012
12	Bright flows on plains	13	200.72	6.53	0.157	0.002	0.376	0.006	1.055	0.015
13	Dark flows on plains	18	181.14	7.65	0.164	0.006	0.382	0.007	1.052	0.015
14	Smooth plains	34	174.92	3.46	0.17	0.005	0.389	0.005	1.059	0.009
15	Lavas of the southwestern slope	6	207.64	5.39	0.158	0.001	0.377	0.004	1.057	0.009
16	Lavas of the slope base	9	181.33	2.4	0.161	0.002	0.382	0.004	1.067	0.006

whole variety of lowland plains is characterized by the highest values of all three color indices. The difference between the lowland plains and the summit plateau is especially noticeable and significant at a confidence level of 99.7%. The increase in the 440/750 nm, 530/750 nm, and 970/750 nm ratios means that the lowland plains are less red, which can be seen simply from the brightness values in the red channel (see table). The lowland plains are lower than the studied areas of the summit plateau by 7–10 km, and, therefore, one may suggest that the color difference is connected either with the difference in the atmospheric thickness above these terrain units or with the dust that is actually redder on the summit plateau than on the lowland plain due to the difference in elevation.

ESTIMATION OF SURFACE AGE FROM CRATER FREQUENCIES

This technique, which has already become a standard one, is described in a number of publications (see, e.g., Hartmann *et al.*, 1981; Neukum and Hiller, 1981; Hartmann *et al.*, 1999; Ivanov, 2001; Neukum *et al.*, 2001). To derive estimates of absolute age from the measured frequencies of craters, we use here the crater chronology model for Mars that combines the efforts of two major research groups in this area (Hartmann and Neukum, 2001). The measurements were made on the HRSC images (a nadir channel), as well as on the MOC images displaying the same regions. The lava-covered areas in the study region were found to vary in age from 20 to 450 Myr with prevailing values of 100–200 Myr (Neukum *et al.*, 2004). In one place, located near the base of the type-3 slope, 15–20 km south-southwest of the triangle mesa described above, the lavas are only

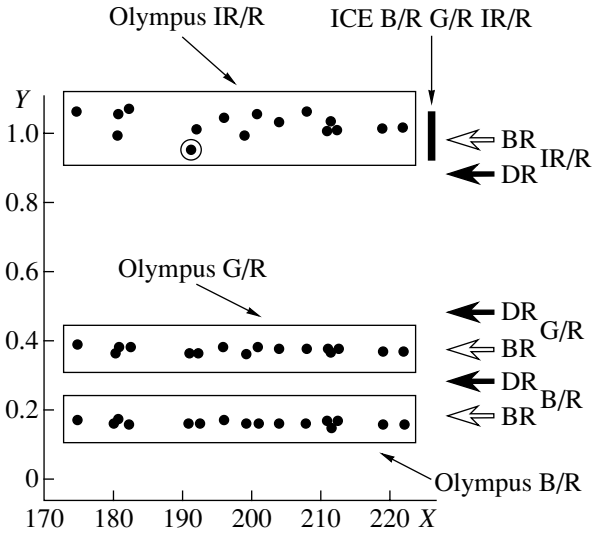

Fig. 21. The diagram presenting the brightness (in DN's, the *X* axis) and color indices (along the *Y* axis) for 16 terrain types of the investigated area. Notation: B/R: 440/750 nm; G/R: 530/750 nm; IR/R: 970/750 nm; BR: bright regions; DR: dark regions of Mars

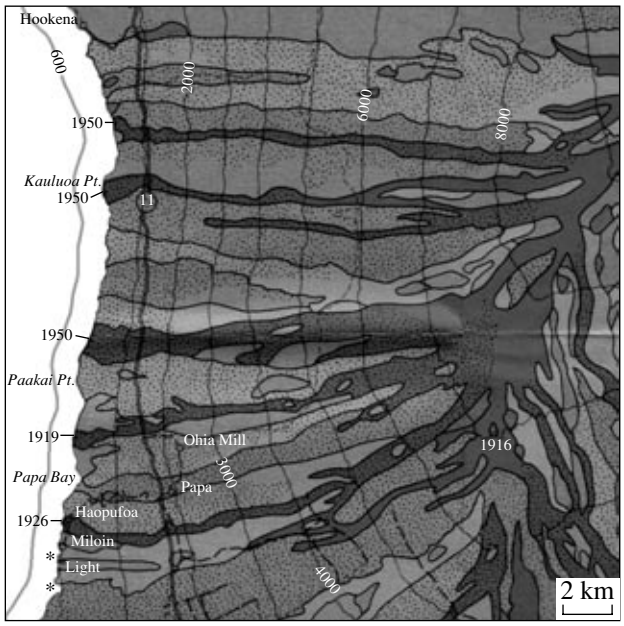

Fig. 22. The lava flows on the southwestern slope of the Mauna Loa volcano, Hawaii. Fragment of the map by Lockwood *et al.* (1988).

2 Myr in age. The northern part of the summit plateau, where lava flows are rare, shows an age close to 50 Myr. The surface of the mesas was found to be very ancient (~3 Gyr) and to contain traces of resurfacing in later epochs. The glacial-type flows vary from 4 to 280 Myr in age (Neukum *et al.*, 2004).

DISCUSSION

The acquired data imply that not only volcanism but also other processes worked in the studied area, which was the western flank of Olympus Mons and the adjacent plains. The lava flows here are similar to those on the slopes of Hawaiian volcanoes in morphology and size (Figs. 3 and 22), which strengthens the interpretation made from the *Mariner 9* and *Viking* data that Olympus Mons is a shield-type basaltic volcano (Carr, 1973; Greeley and Spudis, 1981). The new data also confirm the conclusions drawn from the *Viking* (Lucchitta, 1981) and later from the *Mars Global Surveyor* and *Mars Odyssey* data (Milkovich and Head, 2003), namely, that in the past there were glaciers near the western foot of Olympus Mons that were responsible for specific flows at the slope base (Figs. 10 and 12) and on the plain (Fig. 20). According to celestial mechanics calculations, in past epochs, the inclination of the axis of rotation of Mars to the orbital plain was repeatedly much larger than now (Laskar *et al.*, 2004), which could cause significant evaporation of water on the poles and accumulation of ice in the equatorial regions (Head *et al.*, 2003).

Our analysis of the HRSC images shows that glaciations covered not only the piedmont plains but also at least a part of the edifice summit plateau. In order for glacial valleys (Figs. 8 and 10) to plough the ridge fringing the summit plateau and to cut into the plateau here and there, the ice accumulations supplying these glaciers must have been on the plateau and on the ridge. This is also evidenced by the presence of the fluvial landform described above near the ridge (Fig. 9). The climate models that consider the ice distribution in the equatorial regions of Mars in the epochs of high inclination of the rotational axis of Mars give conflicting results concerning Olympus Mons. For example, in the work by Colaprete *et al.* (2004) modeling the accumulation of ice in those epochs, Olympus Mons appears to be free of ice deposits. At the same time, from the work by Mischna *et al.* (2004) it follows that, at an inclination of the planetary rotation axis of 45°, the thickness of the ice layer in the western part of Olympus Mons could reach tens of centimeters during winter in the northern hemisphere, which could probably result in the formation of glaciers.

The layers outcropping on the summit plateau slopes, on the steep scarps of the slopes of type 1, and on the gentler slopes of type 2 are rather thin, namely, up to 1–2 pixels, which corresponds to 1.5–12 m or 11–22 m for the MOC and HRSC cameras, respectively (Figs. 5–7 and 14). The individual layers are traced to distances of up to 10–15 km, and their thickness is more or less constant. We believe that, if these layers were composed of the basalt flows, which we observe in the studied region (200 m–2 km wide and up to 10–20 km long, usually rimmed), they would be less regular.

In order to verify the above suggestion, we initiated a search of the MOC images that display the lava flows approaching the steep slopes of Olympus Mons, because they can be presumed to compose the upper part of the scarp. Although there are no situations of this kind on the western Olympus slope, about ten MOC images of such situations have been found on the northern, eastern, and southern slopes of the volcano. Figure 23 shows examples of layered rock outcroppings on the steep (up to 30°–35°) slopes. Some of these layers definitely consist of basalt flows (left), and some are composed of the material of the upper part of the summit plateau (right). The layers consisting of lava flows look thicker and less constant in the lateral dimension. Most likely, the material of the mesas, the fringing ridge, and other fine-layered regions of the summit plateau edge is the result of sedimentation of atmospheric dust, possibly volcanic ash (Mouginis-Mark, 2002), and ice rather than lava accumulations. The presence of ice is implied from the above-mentioned specific interaction of the mesa material with inflowing lavas and from the presence of deep rimless depressions within mesas (Fig. 7).

The observations of layered rock outcroppings in the depressions of the upper part of the type-2 slopes (Figs. 13, 14, 16), which are evidently the same as those outcroppings in the scarps of mesas and the ridge, give

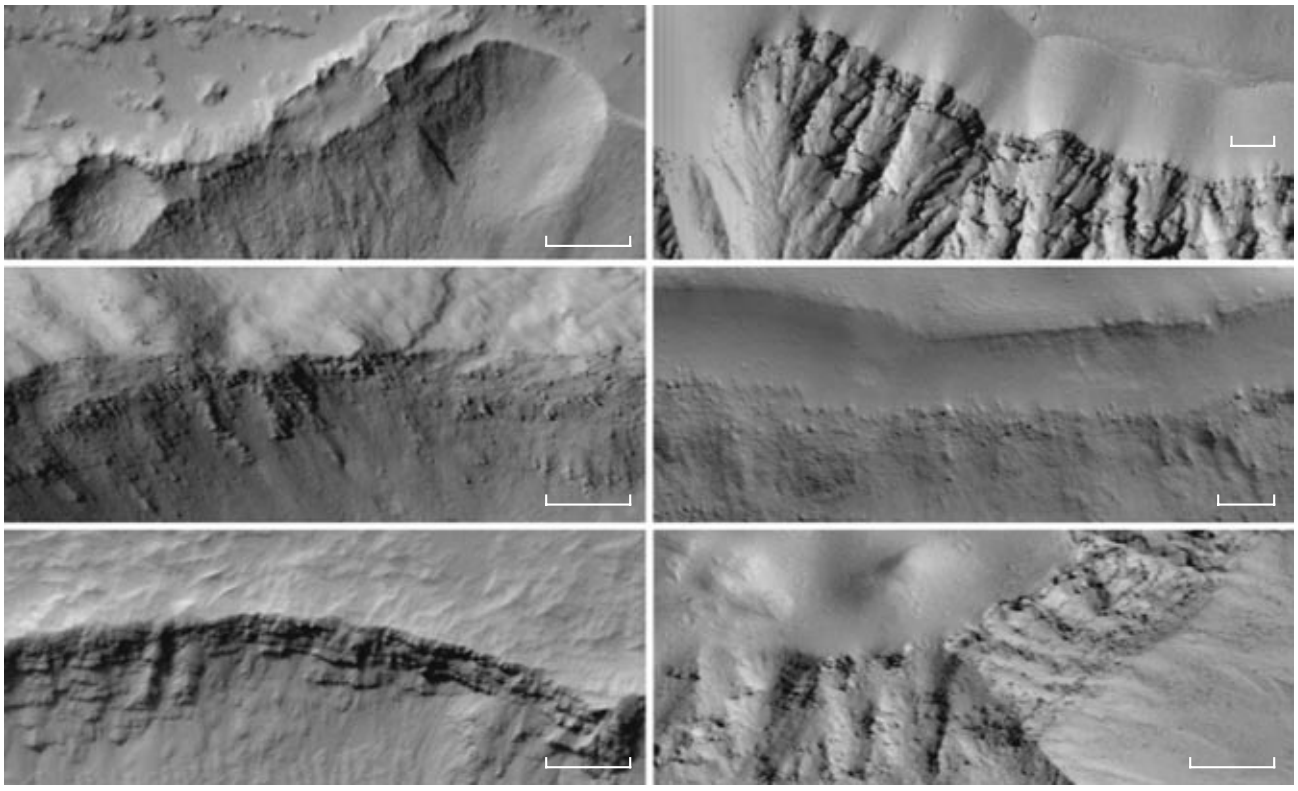

Fig. 23. The layering seen on the steep scarps of Olympus Mons. All images are turned in such a way that the scarp top is at the top of the image. The scale bar is 200 m in all images. Fragments of the MOC images. Left: the layers of lava flows. The flows are seen above the scarp. Top: the southeastern scarp of Olympus Mons, the image M19-01976; middle: the northern scarp, E04-00550; bottom: the southern scarp, M08-05051. Right: the layering of the material composing the mesas and edging ridge. Top: the northern slope of the pentagonal mesa, M20-01387; middle: the northern slope of the polygonal mesa, E04-01135; bottom: the western slope of the edging ridge in its southern part, E05-00061.

additional evidence for their sedimentary (or volcanic–sedimentary) nature and the presence of ice there. These rocks are layered and, judging by the presence of yardangs, easily blown. At the top of the type-2 slopes, they contain well-developed flat-bottom depressions, which are very likely deflation depressions. On the upper part of the slopes of type 2, there are also chaos-like depressions, downslope-extending chains of rimless craters, and channel-like landforms. If the chaoses and crater chains are the collapse depressions of the surface, which seems evident, the following explanation suggests itself: they resulted from the melting of ice contained in the layered rocks above the magmatic dikes, and the channels are the traces of erosion produced in the melting of ice by water.

It turns out that the Olympus Mons edifice in the studied terrain is composed of not only lavas but also sedimentary and volcanic–sedimentary rocks consisting of dust and, probably, volcanic ash and ice. Probably, the water ice is still in these rocks covered with a dust mantle. The presence of dust covering almost the whole surface there follows from both the color ratios determined in this study and the low values of thermal inertia that were known before for this region (Mellon *et al.*, 2000). Theoretical estimations give evidence that even a thin dust cover can protect the buried ice from sublimation over a long period of time (see, e.g., Skorov *et al.*, 2001).

Observations with a neutron spectrometer onboard the *Mars Odyssey* spacecraft (Feldman *et al.*, 2004) show that the upper 0.5–1 m of the surface layer of the western part of Olympus Mons is enriched with hydrogen (up to 5–6 mass % converted to H_2O). Neutron spectroscopy does not allow the hydrogen state to be distinguished. Under the Martian conditions, it can be both minerals containing H_2O and OH groups and H_2O ice (see, e.g. Boynton *et al.*, 2002; Feldman *et al.*, 2002; Mitrofanov *et al.*, 2002; Basilevsky *et al.*, 2003; Feldman *et al.*, 2004). If it is ice, the measured 5–6 mass % of equivalent water must correspond to 15–18% of ice in volume, which amounts to a substantial portion of the pore space of sedimentary rocks. The suggestion on the presence of ice in the surface material or near-surface rocks of the western part of Olympus Mons and the adjacent plain may be possibly tested in the future by radar sounding with the MARSIS instrument onboard *Mars Express* (Nielsen, 2004).

CONCLUSIONS

The examination of the HRSC images (taken during orbit 143) combined with an analysis of the MOC imagery and MOLA altitude profiles have shown that the Olympus Mons edifice, at least in its western part, is composed of not only lavas but also sedimentary and volcanic–sedimentary rocks consisting of dust, volcanic ash, and, probably, H_2O ice that precipitated from the atmosphere. The obtained data also indicate that the glaciations, the traces of which are known for the western foot of Olympus Mons (Lucchitta, 1981; Milkovich and Head, 2003), probably also covered the gentle upper slopes of the construct. It is probable that the ice is essentially still there, protected from sublimation by a dust blanket. Confirming (or rejecting) its presence is a challenge for the scheduled radar sounding with the MARSIS instrument mounted on the *Mars Express* spacecraft as well.

ACKNOWLEDGMENTS

The authors are grateful to M.A. Kreslavskii, R.O.Kuz'min, A.V. Rodin, and Yu.G. Shkuratov for useful discussions and to U. Wolf, W. Zuschneid, I. Fabel, T. Roatsch, K.-D. Matz, F. Scholten, and K. Gwinner for technical assistance. This study was supported by the German Aerospace Agency (DLR) and the German Science Foundation (DFG).

REFERENCES

Baker, V.R., *The Channels of Mars*, Austin Univ. of Texas Press, 1982.

Baker, V.R., Carr, M.H., Gulick, V.C., *et al.*, Channels and Valley Networks, in *Mars*, Kiefer, H.H., Jakosky, B.M., Snyder, C.W., and Matthews, M.S., Eds., Tuscon: Univ. Arizona Press, 1992, pp. 493–522.

Banin, A., Clark, B.C., and Waenke, H., Surface Chemistry and Mineralogy, in *Mars*, Kiefer, H.H., Jakosky, B.M., Snyder, C.W., and Matthews, M.S., Eds., Tuscon: Univ. Arizona Press, 1992, pp. 594–625.

Basilevsky, A.T., Litvak, M.L., Mitrofanov, I.G., *et al.*, Search for Traces of Chemically Bound Water in the Martian Surface Layer Based on HEND Measurements onboard the 2001 *Mars Odyssey* Spacecraft, *Astron. Vestn.*, 2003, vol. 37, no. 5, pp. 423–434 [*Sol. Syst. Res.* (Engl. Transl.), 2003, vol. 37, no. 5, p. 387].

Bibring, J.-P., Soufflot, A., Berthe, M., *et al.*, OMEGA: Observatoire pour la Mineralogie, l'Eau, les Glaces et l'Activite, *ESA SP-1240*, 2004, pp. 37–49.

Boynton, W.V., Feldman, W.C., and Squyres, S.W., Distribution of Hydrogen in the Near Surface of Mars: Evidence for Subsurface Ice Deposits, *Science*, 2002, vol. 297, pp. 81–85.

Carr, M.H., Volcanism on Mars, *J. Geophys. Res.*, 1973, vol. 78, pp. 4049–4062.

Carr, M., *Water on Mars*, New York: Oxford Univ. Press, 1996.

Carr, M.H., Greeley, R., Blasius, K.R., *et al.*, Some Martian Volcanism Features As Viewed from the Viking Orbiters, *J. Geophys. Res.*, 1977, vol. 82, no. 28, pp. 3985–4015.

Colaprete, A., Haberle, R.M., Montmessin, F., and Scheaffer, J., Numerical Modeling of Glaciers in Martian Paleoclimates, *Lunar Planet. Sci. XXXV*, 2004, Abstract #2149.

Feldman, W.C., Boynton, W.V., Tokar, R.L., *et al.*, Global Distribution of Neutrons from Mars: Results from Mars Odyssey, *Science*, 2002, vol. 297, pp. 75–78.

Feldman, W.C., Mellon, M.T., Maurice, S., *et al.*, Contributions from Hydrated States of $MgSO_4$ To the Reservoir of Hydrogen at Equatorial Latitudes on Mars, *Lunar Planet. Sci. XXXV*, 2004, Abstract #2035.

Greeley, R. and Iversen, J.D., *Wind As a Geological Process*, New York: Cambridge Univ. Press, 1985.

Greeley, R. and Spudis, P.D., Volcanism on Mars, *Rev. Geophys. and Space Phys.*, 1981, vol. 19, pp. 13–41.

Harris, S.A., The Aureole of Olympus Mons, *J. Geophys. Res.*, 1977, vol. 82, pp. 3099–3107.

Hartmann, W.K., Strom, R.G., Grieve, R.A.F., *et al.*, Chronology of Planetary Volcanism by Comparative Studies of Planetary Cratering, *Basaltic Volcanism Study Project. Basaltic Volcanism on the Terrestrial Planets*, New York: Pergamon, 1981, pp. 1049–1127.

Hartmann, W.K., Malin, M., McEwen, A., *et al.*, Evidence for Recent Volcanism on Mars from Crater Counts, *Nature*, 1999, vol. 397, pp. 586–589.

Hartmann, W.K. and Neukum, G., Cratering Chronology and the Evolution of Mars, *Space Sci. Rev.*, 2001, vol. 96, pp. 165–194.

Hauber, E., van Gasselt, S., Ivanov, B., *et al.*, Discovery of Very Young and Glacial Activity at Hecates Tholus, Mars, in *Mars Express* HRSC Images, *Nature*, 2005 (in press).

Head, J.W., Mustard, J.F., Kreslavsky, M.A., *et al.*, Recent Ice Ages on Mars, *Nature*, 2003, vol. 426, pp. 792–802.

Head, J.W., Neukum, G., Jaumann, R., *et al.*, Recent Midlatitude Glaciation on Mars: Evidence for Snow and Ice Accumulation and Flow in *Mars Express* HRSC Data, *Science*, 2005 (in press).

Ivanov, B.A., Mars/Moon Cratering Rate Ratio Estimates, *Space Sci. Rev.*, 2001, vol. 96, pp. 87–104.

Ivanov, M.A. and Head, J.W., Syrtis Major and Isidis Basin Contact: Morphological and Topographic Characteristics of Syrtis Major Lava Flows and Material of the Vastitas Borealis Formation, *J. Geophys. Res.*, 2003, vol. 108, doi 10.1029/2002JE001994.

Laskar, J., Correia, A.C., Gastineau, M., *et al.*, Long Term Evolution and Chaotic Diffusion of the Insolation Quantities of Mars, *Icarus*, 2004, vol. 170, pp. 343–364.

Lockwood, J.P., Lipman, P.W., and Petersen, L.D., Generalized Ages of Surface Lava Flows of Mauna Loa Volcano, Hawaii, in *USGS Miscellaneous Investigation Series Map I-1908*, 1988.

Lopes, R., Hiller, K., Neukum, G., and Guest, J.E., Further Evidence of the Olympus Mons Aureole, *J. Geophys. Res.*, 1982, vol. 87, pp. 9917–9928.

Lucchitta, B.K., Mars and Earth: Comparison of Cold Climate Features, *Icarus*, 1981, vol. 45, pp. 264–303.

McCord, T., Jaumann, R., Hoffmann, H., *et al.*, The Color Capabilities of the Mars Express High Resolution Stereo

Camera, *Europ. Geophys. Union Gen. Assembly I*, 2004, Abstract EGU04-A-06358.

Mellon, V.T., Jakosky, B., Kieffer, H., and Christensen, P., High Resolution Thermal Inertia Mapping from the Mars Global Surveyor Thermal Emission Spectrometer, *Icarus*, 2000, vol. 148, pp. 437–455.

Milkovich, S.M. and Head, J.W., Olympus Mons fan-shaped deposit morphology: Evidence for debris glaciers, *6th International Mars Conf.*, 2003, Abstract #3149.

Mischna, M.A., Richardson, M.I., Wilson, R.J., and Zent, A., Explaining the Mid-Latitude Ice Deposits with a General Circulation Model, *Lunar Planet. Sci. XXXV*, 2004, Abstract #1861.

Mitrofanov, I., Anfimov, D., Kozyrev, A., *et al.*, Maps of Subsurface Hydrogen from High Energy Neutron Detector, *Science*, 2002, vol. 297, pp. 78–81.

Morris, E.C., Aureole Deposits of the Martian Volcano Olympus Mons, *J. Geophys. Res.*, 1982, vol. 87, pp. 1164–1178.

Mouginis-Mark, P.J., Prodigious Ash Deposits Near the Summit of Arsia Mons Volcano, Mars, *Geophys. Rev. Lett.*, 2002, vol. 29, no. 16.10.1029/2002GL015296.

Murray, J.B., Muller, J.P., Neukum, G., *et al.*, Evidence from the *Mars Express* High Resolution Stereo Camera for a Frozen Sea close to Mars' Equator, *Nature*, 2005 (in press).

Neukum, G. and Hiller, K., Martian Ages, *J. Geophys. Res*., 1981, vol. 86, pp. 3097–3121.

Neukum, G., Ivanov, B.A., and Hartmann, W.K., Cratering Record in the Inner Solar System in Relation To the Lunar Reference System, *Space Sci. Rev.*, 2001, vol. 96, pp. 55–86.

Neukum, G. and Jaumann, R., and the HRSC Co-Investigator and Experiment Team, HRSC: The High Resolution Stereo Camera of Mars Express, *ESA SP-1240*, 2004, pp. 17–35.

Neukum, G., Jaumann, R., Hoffmann, H., *et al.*, Mars: Recent and Episodic Volcanic, Hydrothermal, and Glacial Activity Revealed by the *Mars Express* High Resolution Camera (HRSC) experiment, *Nature*, 2005, vol. 432, pp. 971–979.

Nielsen, E., *Mars Express* and MARSIS, *Space Sci. Rev*., 2004, vol. 111, pp. 245–262.

Pieters, C.M. and Englert, P.A.J., Eds., *Remote Geochemical Analysis: Elemental and Mineralogical Composition*, Cambridge: Univ. Press, 1993.

Skorov, Y.V., Markiewicz, W.J., Basilevsky, A.T., and Keller, H.U., Stability of Water Ice Under a Porous Nonvolatile Layer: Implications To the South Polar Layered Deposits of Mars, *Planet. Space Sci*, 2001, vol. 49, pp. 59–63.

Squyres, S.W., Wilhelms, D.E., and Moosman, A.C., Large-Scale Volcano-Ground Ice Interactions on Mars, *Icarus*, 1987, vol. 70, pp. 385–408.

Tanaka, K.L., Ice-Lubricated Gravity Spreading of the Olympus Mons Aureole Deposits, *Icarus,* 1985, vol. 62, pp. 191–206.